

Successive Interference Cancellation for Fiber-Optic Channels with Direct Detection

Tobias Prinz, Daniel Plabst, Thomas Wiegart, Stefano Calabrò, Nobert Hanik, and Gerhard Kramer

Abstract—Two simplified transceiver architectures are studied for fiber-optic links with direct detection and oversampling: separate detection and decoding (SDD) and successive interference cancellation (SIC) with multi-level coding and multi-stage decoding. For bipolar modulation, SIC achieves rates close to those of joint detection and decoding (JDD), thereby achieving large energy gains over SDD and over classic intensity modulation. Gibbs sampling is used to reduce the detector complexity and achieves rates close to those of the forward-backward algorithm. Simulations with polar codes and higher-order modulation confirm the predicted rate and energy gains.

Index Terms—Capacity, direct detection, forward-backward algorithm, Gibbs sampling, polar coded modulation, successive interference cancellation

I. INTRODUCTION

Short-reach fiber-optic communication systems usually use low-cost direct detection (DD) receivers [1] with one photodiode (PD) per wavelength that detects the intensity of the received optical signal. To allow easy reconstruction of the transmitted data, DD receivers are combined with intensity modulation (IM) at the transmitter [2]–[4].

The paper [5] showed that the DD capacity increases by oversampling¹ at the receiver. In fact, if the dominant noise is before DD then the capacity is within 1 bit/s/Hz of the capacity with coherent detection. This motivates DD with bipolar modulation (BM) or even complex-valued modulations [5]–[10]. The paper [10] considers spectrally efficient frequency-domain raised-cosine (FD-RC) pulses and computes achievable rates via the methods in [11] that account for the channel memory. The results show that BM and complex-valued modulations exhibit significant energy gains compared to classic IM. In this paper, we show how to approach the rates from [10] with practical coded modulation schemes.

A. Detection and Decoding

The rates in [10] are achieved with joint detection and decoding (JDD). JDD is usually infeasible because the complexity grows exponentially in the encoder and channel memory. There are several approaches to reduce JDD complexity, and we consider the following classic methods.

Submitted to *IEEE Journal of Lightwave Technology* on December 15, 2022.

T. Prinz, D. Plabst, T. Wiegart, N. Hanik, and G. Kramer are with the Institute for Communications Engineering, Technical University of Munich, 80333 Munich, Germany (e-mail: {tobias.prinz, daniel.plabst, thomas.wiegart, norbert.hanik, gerhard.kramer}@tum.de). S. Calabrò, is with the Huawei Munich Research Center, 80992 Munich, Germany (e-mail: stefano.calabro@huawei.com).

¹The term “oversampling” refers to sampling faster than the symbol rate.

- Separate detection and decoding (SDD): the detector computes symbol-wise *a posteriori* probabilities (APPs) that it passes to a decoder as soft decisions, see [12], [13].
- Turbo detection and decoding (TDD): use SDD but include a turbo loop where soft decisions are passed between the detector and decoder, see [14], [15].
- Successive interference cancellation (SIC): use SDD but with multi-level coding (MLC) and multi-stage detection/decoding (MSD), see [16]–[18].

SDD is suboptimal in general, e.g., channels with memory exhibit a rate loss that grows with the memory, see [19, Fig. 7-9], [17, Fig. 5]. On the other hand, TDD can approach JDD performance by carefully designing codes (e.g., low density parity check (LDPC) codes) with density evolution or extrinsic information transfer (EXIT) charts [20]. The main disadvantage is that one cannot use “off-the-shelf” or standard codes, i.e., the code EXIT curve should be adapted to the detector EXIT curve which depends on the modulation format, detection algorithm, and signal-to-noise ratio (SNR).

The advantages of SIC over SDD and TDD are that, first, one can approach JDD performance and, second, one can do so with off-the-shelf binary codes [17], [18]. Consider the following MLC/MSD example where b^k is a string of k bits b_1, \dots, b_k . Suppose b^k is multiplexed into two strings b^{k_1} and b^{k_2} where $k = k_1 + k_2$. Each string is encoded with a length $n/2$ code and the two codewords are demultiplexed into a length n bit string. The coded bits are mapped to modulation symbols that are transmitted over a channel. The receiver detects and decodes in two stages. The first stage performs SDD for b^{k_1} by computing APPs and passing these to a decoder that provides an estimate \hat{b}^{k_1} . The second stage uses this estimate as *a priori* information to detect and decode b^{k_2} , i.e., the *a priori* information from the first stage increases the achievable rates in the second stage. Of course, MLC/MSD extends to more than two detection and decoding stages [17].

B. Detection Algorithms

SDD requires symbol-wise APPs that can be computed efficiently by the forward-backward algorithm (FBA) [21]. To determine the APP of the i^{th} channel input, the FBA marginalizes a multivariate joint density, see [22, Eq. (11.21)]. Like the Viterbi algorithm, the FBA complexity grows exponentially with the channel memory and its implementation is infeasible for large memory or large symbol alphabets.

To reduce complexity, one can approximate the marginals of high-dimensional multivariate distributions by Markov chain Monte Carlo (MCMC) sampling. We use Gibbs sampling which is a special case of the Metropolis-Hastings algorithm. The method iteratively draws samples from joint posterior

densities that tend to the JDD posterior with the number of iterations [23]. One may then use the samples to estimate the marginal APPs of interest. Gibbs sampling to estimate APPs was proposed in [24]–[27], where the applications were code-division multiple access (CDMA) and multiple-input multiple-output (MIMO) systems. The papers [28]–[32] used Gibbs sampling for channels with intersymbol interference (ISI) and showed that the bit error rate (BER) is only slightly worse than with the FBA.

MCMC sampling can be refined in several ways. For example, the paper [29] uses *importance sampling* to reduce the number of iterations to compute APPs with a desired accuracy. Next, MCMC sampling often “stalls” at high SNR, i.e., many iterations are needed to obtain good APP estimates [33]. Heuristics such as increasing the variance of the channel model can help to improve convergence [34]–[37], i.e., one draws samples from a “mismatched” proposal distribution that differs from the channel model under study. To compute the APPs for the true channel, one may use importance sampling to weight the samples of the proposal distribution [35].

C. Organization

This paper is organized as follows. Sec. II reviews the system model. Sec. III and Sec. IV review the information rates of SDD and SIC, respectively. Sec. V describes SIC for binary forward error control (FEC) codes. Sec. VI reviews Gibbs sampling for APP estimation. Sec. VII reviews achievable rates for SDD and SIC through mismatched decoding. Sec. VIII presents numerical results for SDD and SIC receivers and compares with the plots in [10]. The results show that SDD does not approach the JDD rates in [10] and that the BM rates can be worse than the IM rates. The results also show that SIC with Gibbs sampling recovers most of the gains. Sec. IX concludes the paper and suggests research problems. The Appendix discusses phase ambiguities in symbol-wise APPs for certain modulation alphabets. Differential phase mappings are provided to avoid ambiguous APPs.

D. Notation

Vectors and matrices are written using bold letters. The transpose of the vector \mathbf{a} is written as \mathbf{a}^T . The $n \times 1$ all-zeros vector is $\mathbf{0}_n$ and the $n \times n$ identity matrix is \mathbf{I}_n . We write the element-wise absolute values of the entries in \mathbf{a} as $|\mathbf{a}|$ and the element-wise squares as \mathbf{a}^2 . We use the string notation $x_\kappa^n = (x_\kappa, \dots, x_n)$ and $\mathbf{x}_\kappa^n = (\mathbf{x}_\kappa, \dots, \mathbf{x}_n)$ but omit the subscript if $\kappa = 1$. We write $\mathbf{a}_{\setminus \mathbf{a}'}$ to denote the removal of the entries specified in \mathbf{a}' from \mathbf{a} . For complex-valued x , we write $\angle x$ for the argument (or phase) of x .

The sinc function is defined as $\text{sinc}(t) = \sin(\pi t)/(\pi t)$. The signal $a(t)$ and its Fourier transform $A(f)$ are related by the notation $a(t) \circ \bullet A(f)$. The expression $g(t) * h(t)$ refers to the convolution of $g(t)$ and $h(t)$ and $\|a(t)\|^2 = \int_{-\infty}^{\infty} |a(t)|^2 dt$ is the energy of $a(t)$.

Random variables (RVs) are written with upper case letters and their realizations with lower-case letters. The probability mass function (PMF) or density of a vector of *discrete* or *continuous* RVs \mathbf{X} is written as $P_{\mathbf{X}}$ or $p_{\mathbf{X}}$, respectively.

$\mathbb{E}[f(X, Y)]$ denotes expectation of $f(X, Y)$ with respect to the joint density of X and Y . A multivariate real Gaussian density is written as $\mathcal{N}(\mathbf{x}; \boldsymbol{\mu}, \mathbf{C})$ where $\boldsymbol{\mu}$ and \mathbf{C} are a mean vector and covariance matrix, respectively. The conditional density of \mathbf{Y} given \mathbf{X} is written as $p_{\mathbf{Y}|\mathbf{X}}$. The entropy of a discrete-valued \mathbf{X} and the mutual information of \mathbf{X} and \mathbf{Y} with conditional density $p(\mathbf{y}|\mathbf{x})$ are defined as

$$H(\mathbf{X}) = \mathbb{E}[-\log_2 P(\mathbf{X})] \quad (1)$$

$$I(\mathbf{X}; \mathbf{Y}) = \mathbb{E}\left[\log_2 \frac{p(\mathbf{Y}|\mathbf{X})}{p(\mathbf{Y})}\right] \quad (2)$$

where we measure the quantities in bits. As in (1), we often discard subscripts on PMFs or densities if the arguments are uppercase or lowercase versions of their RVs.

II. SYSTEM MODEL

Propagation in fiber is described by the Nonlinear Schrödinger Equation (NLSE) [38, p. 65], [39, Part 2] that models attenuation and CD, both linear effects, and a Kerr nonlinearity. We are interested in short-reach links where the launch power is sufficiently small so that one may neglect the Kerr non-linearity, and where the system has no optical amplifiers so that one may neglect optical noise.

A. Continuous-Time Model

Consider the continuous-time model in [10] that is depicted in Fig. 1. The symbol alphabet is $\mathcal{A} = \{a_1, \dots, a_M\}$ with $M = 2^m$. A source puts out a sequence of uniformly, independently and identically distributed (u.i.i.d.) symbols $(X_\kappa)_{\kappa \in \mathbb{Z}} = (\dots, X_1, X_2, X_3, \dots)$ with $X_\kappa \in \mathcal{A}$. We perform pulse shaping with $g_{\text{tx}}(t)$ to obtain the baseband waveform

$$X(t) = \sum_{\kappa} X_\kappa \cdot g_{\text{tx}}(t - \kappa T_s) \quad (3)$$

with symbol-rate $B = 1/T_s$. We distinguish two choices for pulse shaping: FD-RC pulses [10, Eq. (5)] with roll-off factor $\alpha > 0$ and the case $\alpha = 0$ for which we obtain the sinc pulse, see [10, Eq. (6)].

The channel exhibits CD with response [40, Sec. II.B]

$$h_L(t) \circ \bullet H_L(f) = e^{j(\beta_2/2)\omega^2 L} \quad (4)$$

where β_2 is the CD parameter, $\omega = 2\pi f$ is the angular frequency and L is the fiber length. The convolution of $X(t)$ and the channel response $h_L(t)$ results in $X_L(t)$.

The receiver PD outputs the intensity $Z'(t) = |X_L(t)|^2$ of the optical signal and we model the PD noise $N'(t)$ by a real-valued white Gaussian random process with two-sided power spectral density $N_0/2$. The noise term might also include noise contributions from an optical transimpedance amplifier (TIA) and the ADC. The signal and noise then pass through a bandwidth-limited sampling device, resulting in $Y(t)$. The corresponding bandwidth-limited filter $g_{\text{rx}}(t)$ has a unit gain brickwall frequency response from $[-B, B]$ that rejects out-of-band signals, see [10, Eq. (9)].

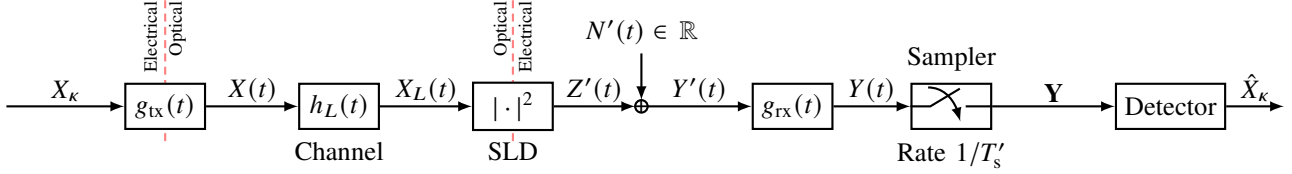


Fig. 1: Communication system with DD [10].

B. Discrete-Time Model

The receiver samples at rate $1/T'_s = 2B$, i.e., the oversampling factor is $N_{os} = T_s/T'_s = 2$ samples per transmit symbol. We next describe the discrete-time model for a FD-RC transmit pulse with roll-off factor $\alpha = 0$, i.e., a sinc pulse. For roll-off factors $\alpha > 0$, we also use this discrete model but ensure that the channel observations are correctly generated, see [10, Eqs. (11)-(12), (60)].

Following the steps in [10, Sec. II. B], consider a receiver that collects $2n$ samples of $Y(t)$ into the vector

$$\mathbf{y} = [y_1, y_2, y_3, \dots, y_{2n}]^T \in \mathbb{R}^{2n \times 1}. \quad (5)$$

The combined response of the transmit pulse and fiber is $\psi(t) = g_{tx}(t) * h_L(t)$ and we define the samples $\psi_k = \psi(kT'_s)$, $k \in \mathbb{Z}$. To illustrate, assume that the channel taps outside an interval $[0, K-1]$ are zero, where K is an odd integer. We write the discrete-time channel Toeplitz matrix as $\Psi \in \mathbb{C}^{2n \times (2n+K-1)}$; this matrix is constructed from the two-fold oversampled channel response $\psi = [\psi_{K-1}, \dots, \psi_0] \in \mathbb{C}^K$, cf. [10, Sec. II. B]. Define the vector of noise-free samples

$$\mathbf{z} = |\Psi \tilde{\mathbf{x}}'|^{o2} = [z_1, z_2, z_3, \dots, z_{2n}]^T \in \mathbb{R}^{2n \times 1} \quad (6)$$

with input vector $\tilde{\mathbf{x}}' = [\mathbf{s}_0^T, (\mathbf{x}')^T]^T$ and upsampled symbols

$$\mathbf{x}' = [0, x_1, 0, x_2, \dots, 0, x_n]^T \in \mathbb{C}^{2n \times 1} \quad (7)$$

where the initial state vector is

$$\mathbf{s}_0 = [0, x_{1-\tilde{K}}, 0, x_{2-\tilde{K}}, \dots, 0, x_0]^T \in \mathbb{C}^{(K-1) \times 1} \quad (8)$$

and the channel memory is $\tilde{K} = (K-1)/2$. The channel state \mathbf{s}_0 is assumed to be known at the receiver. The discrete-time channel can be described by a conditional Gaussian density with mean zero and variance $\sigma_N^2 = N_0B$:

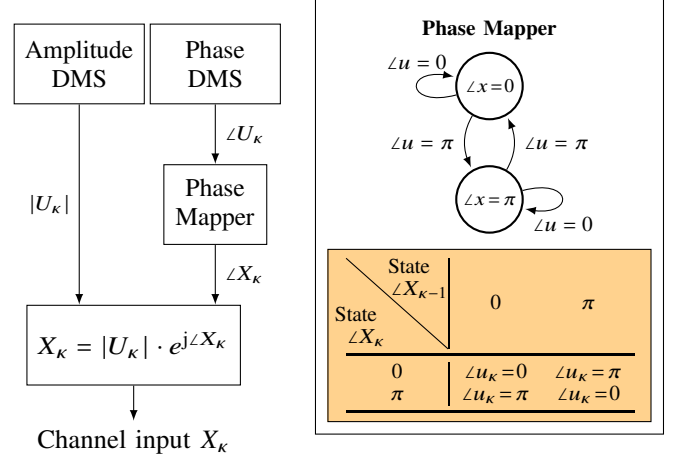
$$p(\mathbf{y}|\mathbf{x}) = \mathcal{N}(\mathbf{y} - |\Psi \tilde{\mathbf{x}}'|^{o2}; \mathbf{0}_{2n}, \sigma_N^2 \mathbf{I}_{2n}). \quad (9)$$

III. SDD RECEIVERS

This section describes SDD receivers for ISI channels and reviews their information rates, see [19].

A. Separate Detection and Decoding

Practical receivers usually use SDD. The detector computes symbol-wise APPs $P(x_k|\mathbf{y})$, $k = 1, \dots, n$, which are passed to a decoder that makes decisions on the transmitted data. The decoder usually operates with a binary interface and computes bit-wise APPs, also called bit-wise metrics, by marginalizing the symbol-wise APPs $P(x_k|\mathbf{y})$.

Fig. 2: Differential phase mapper example for M -ASK.

B. Differential Phase Coding

The PD causes the symbol-wise APPs to have phase ambiguities for certain modulation alphabets with symmetries, see the Appendix. As suggested in [10], differential phase coding can mitigate the phase ambiguities, i.e., we add phase encoding as shown in Fig. 2 for the special case of two phases ($0, \pi$). The state transition diagram and table in Fig. 2 illustrate the relationship between the current state $\angle X_k$ and the last state $\angle X_{k-1}$ given the input $\angle U_k$, see [41, Sec. 2.3]. Let $\angle x_0 = 0$ be the initial state of the phase mapper. We describe the differential phase encoding by

$$\mathbf{X} = f_{\text{diff}}(\mathbf{U}) \quad (10)$$

where $f_{\text{diff}}(\cdot)$ leaves the amplitudes unchanged and applies a phase mapping to $\angle \mathbf{U}$ according to Fig. 2. One can extend differential phase encoding to constellations with more than two phases, see [39, Sec. IV.B] or [8, Fig. 8]. Note that we also apply differential phase coding for SIC, see Sec. IV.

C. Achievable Rates

For n transmit symbols \mathbf{U} , define the entropy rate, conditional entropy rate and mutual information rate in bits per transmitted symbol as the respective

$$H_n(\mathbf{U}) = \frac{1}{n} H(\mathbf{U}) \quad (11)$$

$$H_n(\mathbf{U}|\mathbf{Y}) = \frac{1}{n} H(\mathbf{U}|\mathbf{Y}) \quad (12)$$

$$I_n(\mathbf{U}; \mathbf{Y}) = H_n(\mathbf{U}) - H_n(\mathbf{U}|\mathbf{Y}). \quad (13)$$

Consider the lower bound

$$I_n(\mathbf{U}; \mathbf{Y}) = H_n(\mathbf{U}) - H_n(\mathbf{U}|\mathbf{Y}) \quad (14)$$

$$\geq H_n(\mathbf{U}) - \frac{1}{n} \sum_{\kappa=1}^n H(U_\kappa|\mathbf{Y}) \quad (15)$$

$$:= I_{n,\text{SDD}}$$

with equality if U_κ and $U^{\kappa-1}$ are conditionally independent given \mathbf{Y} . The limiting rates of (14) and (15) are

$$I(\mathcal{U}; \mathcal{Y}) = \lim_{n \rightarrow \infty} H_n(\mathbf{U}) - H_n(\mathbf{U}|\mathbf{Y}) \quad (16)$$

$$I_{\text{SDD}} = \lim_{n \rightarrow \infty} H_n(\mathbf{U}) - \frac{1}{n} \sum_{\kappa=1}^n H(U_\kappa|\mathbf{Y}) \quad (17)$$

and these quantities exist for stationary signalling. From (14) and (15) it follows that

$$I_{\text{SDD}} \leq I(\mathcal{U}; \mathcal{Y}). \quad (18)$$

The rate $I(\mathcal{U}; \mathcal{Y})$ is achievable using JDD. For example, for linear codes JDD can be implemented by a Viterbi algorithm on a *super-trellis*, i.e., the trellis states are the direct product of the linear encoder states [21] and the channel states, see [42]–[44]. JDD is often infeasible because the complexity grows exponentially in the encoder and channel memory, and in practice one uses SDD with rate I_{SDD} [19, Sec. IV].

For channels with *memory*, the difference between $I(\mathcal{U}; \mathcal{Y})$ and I_{SDD} may be significant at intermediate-to-high SNRs, see [19, Figs. 7-9], [45, Fig. 12]. The reason is that SDD provides only posterior *marginals* to the channel decoder, thereby neglecting stochastic dependencies. The rate loss increases with the channel memory in general [19, Figs. 7-9].

IV. SUCCESSIVE INTERFERENCE CANCELLATION (SIC)

This section reviews SIC and the corresponding rates as described in [17], [18]. SIC first performs a serial-to-parallel (S/P) conversion on the information symbols \mathbf{U} , i.e., down-sample \mathbf{U} by a factor of S to create S shorter strings of length $\Gamma = n/S$ (assume that Γ is an integer). We write

$$\begin{aligned} \mathbf{V}_s &= (U_s, U_{s+S}, U_{s+2S} \dots) = (U_{s+(t-1)S})_{t=1}^\Gamma \\ &:= (V_{s,t})_{t=1}^\Gamma, \quad s = 1, \dots, S \end{aligned} \quad (19)$$

and we stack these vectors to form the vector $\mathbf{V} = (\mathbf{V}_s)_{s=1}^S$. Fig. 3a illustrates the S/P conversion.

We clearly have $I_n(\mathbf{U}; \mathbf{Y}) = I_n(\mathbf{V}; \mathbf{Y})$ so consider the bounds

$$I_n(\mathbf{V}; \mathbf{Y}) \stackrel{(a)}{=} H_n(\mathbf{V}) - \frac{1}{n} \sum_{s=1}^S H(\mathbf{V}_s|\mathbf{Y}, \mathbf{V}_1^{s-1}) \quad (20)$$

$$\stackrel{(b)}{\geq} \underbrace{H_n(\mathbf{V}) - \frac{1}{n} \sum_{s=1}^S \sum_{t=1}^\Gamma H(V_{s,t}|\mathbf{Y}, \mathbf{V}_1^{s-1})}_{:= I_{n,\text{SIC}}} \quad (21)$$

$$\stackrel{(c)}{\geq} \underbrace{H_n(\mathbf{V}) - \frac{1}{n} \sum_{s=1}^S \sum_{t=1}^\Gamma H(V_{s,t}|\mathbf{Y})}_{= I_{n,\text{SDD}}} \quad (22)$$

where step (a) follows from the chain rule of entropy; steps (b)-(c) follow because conditioning cannot increase entropy; and step (c) recovers the SDD rate since the double sum runs over all (re-ordered) transmit symbols. The limiting rate

$$I_{\text{SIC}} = \lim_{n \rightarrow \infty} I_{n,\text{SIC}} \quad (23)$$

exists for stationary signalling.

We describe some properties of the SIC rates. First, we can rewrite (21) as

$$I_{n,\text{SIC}} = \frac{1}{S} \sum_{s=1}^S \underbrace{\frac{1}{\Gamma} \sum_{t=1}^\Gamma (H(V_{s,t}) - H(V_{s,t}|\mathbf{Y}, \mathbf{V}_1^{s-1}))}_{:= I_{n,\text{SIC}}^{(s)}}. \quad (24)$$

The expression (24) suggests the receiver architecture in Fig. 4 that has S stages where every stage has a symbol-wise APP detector and decoder. Note that SDD is a special case of SIC with $S = 1$. In SIC stage s , the detector computes APPs

$$P(v_{s,t}|\mathbf{y}, \hat{\mathbf{v}}_1^{s-1}), \quad t = 1, \dots, \Gamma \quad (25)$$

where $\hat{\mathbf{v}}_1^{s-1}$ are decoded estimates from previous stages.

Next, suppose \mathbf{V}_s is encoded with a code rate smaller than the limiting rate [17, Sec. III a)]

$$I_{\text{SIC}}^{(s)} = \lim_{n \rightarrow \infty} I_{n,\text{SIC}}^{(s)}. \quad (26)$$

This allows reliable transmission of \mathbf{V}_s as the block length tends to infinity. We therefore assume $\mathbf{V}_s = \hat{\mathbf{V}}_s$ and thus no error propagation occurs between stages. Since each stage uses error-free information from previous stages, the rates of the individual stages are non-decreasing

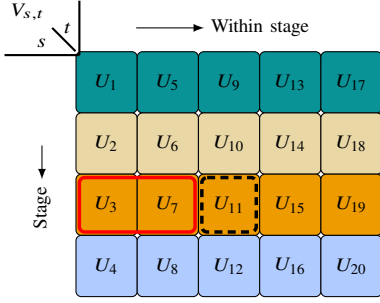
$$I_{\text{SIC}}^{(1)} \leq I_{\text{SIC}}^{(2)} \leq \dots \leq I_{\text{SIC}}^{(S)}. \quad (27)$$

By (22) we have $I_{\text{SDD}} \leq I_{\text{SIC}}$, i.e., SIC outperforms SDD.

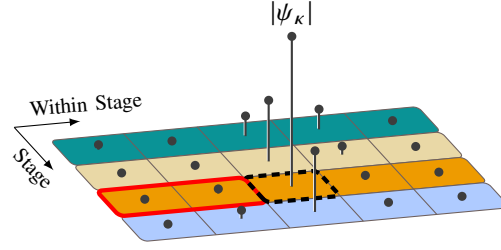
By (20) and (21) we have $I_{\text{SIC}} \leq I(\mathcal{U}; \mathcal{Y})$ and the number of decoding stages S affects the accuracy of this bound. Note that (21) holds with equality if $V_{s,t}$ and $(V_{s,i})_{i=1}^{t-1}$ are conditionally independent given \mathbf{Y} and \mathbf{V}_1^{s-1} .

Fig. 3 shows how SIC reduces the effective ISI for an input string U^{20} with $S = 4$, $\Gamma = 5$. For example, consider detection of $V_{3,3} = U_{11}$ for which the channel causes ISI as illustrated in Fig. 3b. As S increases, symbols in the same stage such as (U_3, U_7) become less relevant when detecting U_{11} , i.e., the S/P conversion reduces the impact of $(V_{s,i})_{i=1}^{t-1}$ on $V_{s,t}$. And this reduces that rate loss between (20) and (21). To limit complexity, the number of stages should thus be chosen based on the channel memory.

One disadvantage of SIC as compared to SDD and TDD is that the component codes are shorter due to the stages (alternatively, the decoding latency increases if one uses the same code lengths as for SDD or TDD). Moreover, one must back-off from the rate (26) as the block length decreases [46], [47] and the back-off can make the SIC gain vanish. To mitigate this effect, we use polar codes with successive cancellation list decoding (SCL) [48] where the list is passed across decoding stages [49], [50], see Sec. VIII-B.



(a) S/P conversion of an input string U^{20} to $V_{s,t}$, $s = 1, \dots, 4$ and $t = 1, \dots, 5$.



(b) Effective ISI with SIC.

Fig. 3: SIC example.

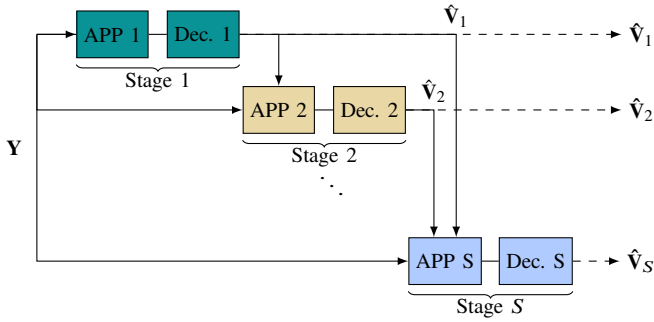


Fig. 4: SIC decoder.

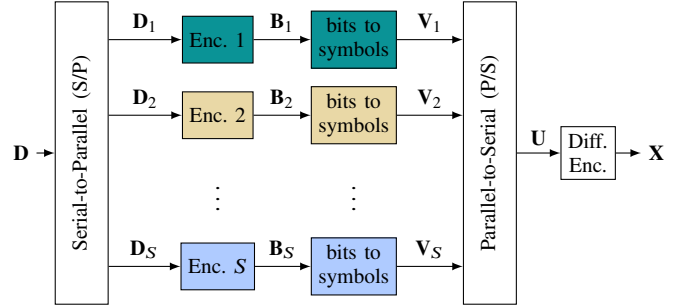


Fig. 5: SIC encoder for binary codes.

V. BINARY CODES FOR SIC

This section shows how SIC can be combined with binary codes. Each symbol V_k of \mathbf{V} is labeled by m bits denoted by $b(V_k)$. The binary representation of \mathbf{V} with $n \cdot m$ bits is

$$\mathbf{B} = b(\mathbf{V}) = (b(V_1), b(V_2), \dots, b(V_n)). \quad (28)$$

We write $b_l(V_k)$ for the l^{th} bit of V_k . The string of l^{th} bits of \mathbf{V} is $b_l(\mathbf{V}) = (b_l(V_1), \dots, b_l(V_n))$ and has length n .

A. SIC Transmitter

Fig. 5 shows the encoding scheme for SIC with S stages. A binary source provides $k \leq n \cdot m$ independent and uniformly distributed bits \mathbf{D} . We partition \mathbf{D} into S strings $\mathbf{D}_1, \dots, \mathbf{D}_S$ where the length k_s of \mathbf{D}_s can be chosen differently for each s . Each \mathbf{D}_s is encoded to a length Γm bit string \mathbf{B}_s , so the code rate per stage is $k_s/(\Gamma m)$. The bits \mathbf{B}_s are mapped to the length Γ string \mathbf{V}_s of symbols from the modulation alphabet \mathcal{A} . The information rate in bits per channel use (bpcu) for SIC stage s is

$$R_s = \frac{k_s}{\Gamma} \text{ [bpcu]} \quad (29)$$

and the overall information rate is k/n bpcu which corresponds to the average rate per stage:

$$R_{\text{SIC}} = \frac{1}{S} \sum_{s=1}^S R_s \text{ [bpcu]}. \quad (30)$$

Finally, the symbol strings $\mathbf{V}_1, \dots, \mathbf{V}_S$ are passed to a P/S converter that reverses (19) and produces \mathbf{U} .

B. SIC Receiver

We next describe how binary decoders may incorporate *symbol-wise* APPs. Two common choices are bit-metric decoding [51], [52] and MLC/MSD [16], [53]. We focus on binary MLC/MSD.

Replacing $V_{s,t}$ by $b(V_{s,t})$, we rewrite (24) as

$$\begin{aligned} I_{n,\text{SIC}} &= I_{n,\text{MSD}} \\ &= \frac{1}{S} \sum_{s,l} \frac{1}{\Gamma} \sum_t \underbrace{(H(b_l(V_{s,t})) - H(b_l(V_{s,t})|\mathbf{Y}, \mathbf{V}_1^{s-1}, b_i(V_{s,t})_{i=1}^{l-1}))}_{:= I_{n,\text{MSD}}^{(s,l)}} \end{aligned} \quad (31)$$

where $I_{n,\text{MSD}}^{(s,l)}$ is the information rate of bit level l in SIC stage s . Binary MSD has m decoding stages and works successively through the bit levels. Decoding stage l computes the *conditional* APP of bit level l :

$$P(b_l(v_{s,t})|\mathbf{y}, \hat{\mathbf{v}}_1^{s-1}, (\hat{b}_i(v_{s,t})_{i=1}^{l-1}), \quad l = 1, \dots, m \quad (32)$$

where $(\hat{b}_i(v_{s,t})_{i=1}^{l-1})$ are the bit estimates from the previous $l-1$ bit levels of $V_{s,t}$, and given the symbol estimates $\hat{\mathbf{V}}_1^{s-1}$ from previous SIC stages. The APPs are passed to a decoder and

the resulting MAP bit estimate $\hat{b}_l(V_{s,t})$ is passed to the next decoding stage.

Encoding the bit levels $b_l(V_{s,t})$ with code rate smaller than

$$I_{\text{MSD}}^{(s,l)} = \lim_{n \rightarrow \infty} I_{n,\text{MSD}}^{(s,l)} \quad (33)$$

allows reliable transmission of $b_l(V_{s,t})$ as the block length tends to infinity. By successively decoding over the bit-levels $l = 1, \dots, m$ and SIC stages $s = 1, \dots, S$, we assume that no error propagation occurs and $\hat{b}_l(V_{s,t}) = b_l(V_{s,t})$ and $\hat{\mathbf{V}}_1^{s-1} = \mathbf{V}_1^{s-1}$. For large block lengths, MSD achieves the rate I_{SIC} in (23). For MLC/MSD, the transmitter uses a length Γ code for every SIC stage and for every bit-level, i.e., each of the encoding blocks in Fig. 5 has m encoders.

VI. ESTIMATING APPS VIA GIBBS SAMPLING

The FBA [21] can efficiently compute the SDD APPs $P(v_{s,t}|\mathbf{y})$ needed for (22) and the SIC APPs $P(v_{s,t}|\mathbf{y}, \hat{\mathbf{v}}_1^{s-1})$ needed for (21). However, the complexity of the FBA increases exponentially in the channel memory \tilde{N} and becomes prohibitive when $\tilde{N} \gg 1$. To reduce complexity, we use Gibbs sampling [23, Chap. 29.5] to walk through permutations of transmitted strings to generate samples from high-dimensional distributions, e.g., the joint densities $P(\mathbf{v}|\mathbf{y})$ or $P(\mathbf{v}_s|\mathbf{y}, \hat{\mathbf{v}}_1^{s-1})$. The marginal densities $P(v_{s,t}|\mathbf{y})$ or $P(v_{s,t}|\mathbf{y}, \hat{\mathbf{v}}_1^{s-1})$ may be estimated through these samples. Gibbs sampling is an iterative algorithm and as the number of iterations tends to infinity, the required APPs can be estimated as accurately as desired. Likewise, the APPs (32) for SIC with MSD may be computed by Gibbs sampling.

A. Gibbs Sampling Algorithm with SIC

We use bit-wise Gibbs sampling [33], [54] to estimate the APPs (32). The algorithm is explained using the example of $m = 1$, i.e., binary transmit symbols. In SIC stage s , we wish to compute $P(b(v_{s,t})|\mathbf{y}, b(\hat{\mathbf{v}}_1^{s-1}))$ for all $t = 1, \dots, \Gamma$ and provide a decoded estimate $\hat{\mathbf{V}}_s$ to the next SIC stage.

A Gibbs sampler generates samples from a *joint* density by drawing *samples* iteratively from conditional distributions that are easy to sample from. Let $b(\hat{\mathbf{V}}_1^{s-1})$ be the decoded bits from the previous $s - 1$ SIC stages and let

$$\underline{\mathbf{B}} = (\underline{B}_1, \dots, \underline{B}_W) := \mathbf{B}_{\setminus b(\hat{\mathbf{v}}_1^{s-1})} \quad (34)$$

be the remaining W bits that are ordered according to the symbols in the sequence \mathbf{U} .

We wish to generate samples from the joint posterior density of these remaining bits, namely

$$\Phi(\underline{\mathbf{b}}) := P(\underline{\mathbf{b}}|\mathbf{y}, b(\hat{\mathbf{v}}_1^{s-1})). \quad (35)$$

At iteration $i = 0$ we generate a realization of u.i.i.d. bits $\underline{\mathbf{b}}(0)$ to initialize the Gibbs sampler. At iteration i , $i \geq 1$,

the sampler works successively through the bits and draws realizations from the conditional distributions:

$$\underline{\mathbf{b}}(i) \triangleq \begin{cases} \underline{b}_1(i) & \sim \Phi(\underline{b}_1|\underline{b}_2^W(i-1)) \\ \underline{b}_2(i) & \sim \Phi(\underline{b}_2|\underline{b}_1(i), \underline{b}_3^W(i-1)) \\ \vdots & \\ \underline{b}_w(i) & \sim \Phi(\underline{b}_w|\underline{b}_1^{w-1}(i), \underline{b}_{w+1}^W(i-1)) \\ \vdots & \\ \underline{b}_W(i) & \sim \Phi(\underline{b}_W|\underline{b}_1^{W-1}(i)). \end{cases} \quad (36)$$

Observe that each step uses samples from previous steps. The algorithm stops after N_{iter} iterations, and for $N_{\text{iter}} \rightarrow \infty$ the distribution of $\underline{\mathbf{b}}(N_{\text{iter}}), \underline{\mathbf{b}}(N_{\text{iter}}+1), \dots$ tends to $\Phi(\underline{\mathbf{b}})$ [23, Chap. 29.5]. The expression for the conditionals (36) is

$$\Phi(\underline{b}_w|\underline{b}_1^{w-1}(i), \underline{b}_{w+1}^W(i-1)) = \frac{1}{A_1} p(\mathbf{y}|\mathbf{x}(\underline{b}_w)) \quad (37)$$

with symbols

$$\mathbf{x}(\underline{b}_w) = f_{\text{diff}}(b(\hat{\mathbf{V}}_1^{s-1}), \underline{b}_1^{w-1}(i), \underline{b}_w, \underline{b}_{w+1}^W(i-1)) \quad (38)$$

depending on the bit \underline{b}_w and where the normalization constant $A_1 = \sum_{\underline{b}_w} \Phi(\underline{b}_w|\cdot)$ ensures that (37) is a valid PMF. When using $f_{\text{diff}}(\cdot)$ with binary inputs, we place a bit-to-symbol mapping before the differential phase coding. One may readily compute and sample from the univariate PMF (37) because the channel (9) is conditionally Gaussian.

Gibbs sampling for MLD/MSD with $m > 1$ must include the previous bit levels in the conditioning. We next show how to estimate the APPs $\Phi(\underline{b}_w)$ from the $\underline{\mathbf{b}}(0), \dots, \underline{\mathbf{b}}(N_{\text{iter}})$.

B. APP Estimation from MCMC strings

There are several approaches to compute APPs from MCMC sample strings, including empirical density estimation [29, Eq. (25)] and importance sampling [29, Eq. (13)], [35, Sec. III]. The bit-wise APPs are given by

$$\Phi(\underline{b}_w) = \sum_{\underline{\mathbf{b}}_{\setminus \underline{b}_w}} \Phi(\underline{\mathbf{b}}) = \mathbb{E} \left[\Phi(\underline{b}_w|\underline{\mathbf{B}}_{\setminus \underline{b}_w}) \right]. \quad (39)$$

However, computing this marginalization is often infeasible and we approximate (39) by using MCMC sampling. Define

$$\underline{\mathbf{b}}_{\setminus \underline{b}_w}(i) = (\underline{b}_1^{w-1}(i), \underline{b}_{w+1}^W(i-1)) \quad (40)$$

for the sample string without the w^{th} bit. A simple estimate of (39) is

$$\Phi(\underline{b}_w) \approx \frac{1}{N_{\text{iter}}} \sum_{i=1}^{N_{\text{iter}}} \Phi(\underline{b}_w|\underline{\mathbf{b}}_{\setminus \underline{b}_w}(i)) \quad (41)$$

where the strings $\underline{\mathbf{b}}(i)$ are provided by the Gibbs sampler. At low SNR, the estimate (41) is accurate and achieves near-MAP performance [29]. However, at intermediate-to-high SNR the estimates (41) can be inaccurate if the sampling stalls [29], [35], [37]. Stalling occurs when the conditionals (36) are overconfident, e.g., due to poor initialization or a bad current state of the Gibbs sampler.

For example, consider $\Phi(\underline{b}_w = 0|\cdot) \approx 1$ and $\Phi(\underline{b}_w = 1|\cdot) \approx 0$ so the iterations in (36) are nearly deterministic. In this case,

a large N_{iter} is required to obtain good APP estimates. The literature proposes several approaches to address this problem. For example, one may use several Gibbs samplers in parallel that are initialized with different random bit strings [29]. This makes stalling less likely but parallel samplers add computational complexity.

To avoid stalling, we follow [35, Sec. III] and adjust the confidence of the conditionals by adjusting the variance σ_N^2 of the channel likelihood. This approach is also used in [29], [34], [55]. Consider sampling from a modified joint posterior density

$$\Omega(\mathbf{b}) = \frac{1}{A_2} p(\mathbf{y}|\mathbf{b}, b(\hat{\mathbf{v}}_1^{s-1}))^{\frac{1}{\eta}} \quad (42)$$

where the channel likelihood is adjusted by the confidence parameter $\eta \in [1, \infty)$ and A_2 is a normalization constant. In case of a conditionally Gaussian channel, η is a multiplicative factor for the noise variance. As η grows, the conditionals become less confident. Setting $\eta = 1$ recovers (37). The conditionals of (42) needed for Gibbs sampling are:

$$\Omega(\underline{b}_w | \underline{b}_1^{w-1}(i), \underline{b}_{w+1}^w(i-1)) = \frac{1}{A_3} (p(\mathbf{y}|\mathbf{x}(\underline{b}_w)))^{\frac{1}{\eta}} \quad (43)$$

where A_3 is again a normalization constant. We may insert the modified conditionals (43) into (36). As $N_{\text{iter}} \rightarrow \infty$ the distribution of $\mathbf{b}(N_{\text{iter}}), \mathbf{b}(N_{\text{iter}}+1), \dots$ tends to $\Omega(\mathbf{b})$. We use *importance sampling* (see e.g., [23, Chap. 29.2]) to estimate (39) as:

$$\Phi(\underline{b}_w) \approx \frac{1}{N_{\text{iter}}} \sum_{i=1}^{N_{\text{iter}}} \underbrace{\frac{\Phi(\mathbf{b}_{\underline{b}_w}(i))}{\Omega(\mathbf{b}_{\underline{b}_w}(i))}}_{\text{Importance weights}} \Phi(\underline{b}_w | \mathbf{b}_{\underline{b}_w}(i)) \quad (44)$$

where $\mathbf{b}(i)$ are provided by the Gibbs sampler and approximate $\Omega(\mathbf{b})$ and not the true posterior density. The mismatch is resolved by the importance weights. For $\eta = 1$, (44) becomes (41). For $\eta > 1$, stalling is avoided at intermediate-to-high SNR and the estimate (44) is significantly better than (41) in general [35, Fig. 2]. Finally, one may optimize the scaling parameter η for every SNR, e.g., by a line search with the corresponding rate expression as the cost function.

C. SIC with Blocks of Bits (b-SIC)

We next show that practical receivers should compute a modified version of (32) to speed up computation. Consider SDD ($S = 1$) with a 4-ary alphabet and $m = 2$ bit levels. Suppose we use Gibbs sampling to compute the APPs (32) for the first ($l = 1$) bit-level of each symbol. For the second ($l = 2$) bit-level, we must compute

$$P(b_2(v_{1,t})|\mathbf{y}, \hat{b}_1(v_{1,t})), \quad t = 1, \dots, n. \quad (45)$$

For each $t = 1, \dots, n$, we need a complete Gibbs run where bit $\hat{b}_1(V_{1,t})$ is held fixed. This drastically increases complexity.

We thus modify (32) to compute bit-wise APPs conditioned on previous bit levels of all symbols contained in the current SIC stage, i.e., we remove the t -dependent conditioning:

$$P(b_l(v_{s,t})|\mathbf{y}, \hat{\mathbf{v}}_1^{s-1}, \hat{b}_i(\mathbf{v}_s)_{i=1}^{l-1}). \quad (46)$$

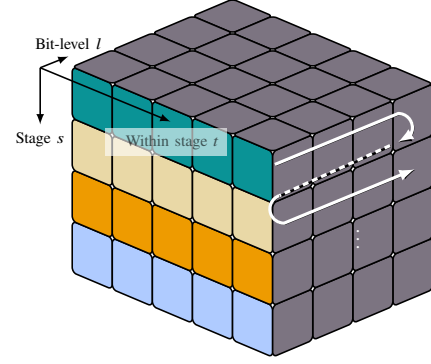


Fig. 6: SIC with $m = 4$ bit levels.

Algorithm	Multiplications per Iteration	Iterations
FBA	$\mathcal{O}(n \cdot S \cdot \mathcal{A} ^{\tilde{N}})$	1
Gibbs (b-SIC)	$\mathcal{O}(n \cdot S \cdot \tilde{N}^2 \cdot N_{\text{par}})$	60

TABLE I: Algorithmic complexity for a mismatched channel of memory \tilde{N} .

SIC with the modified detector (46) is illustrated in Fig. 6 and iterates successively through blocks of T bits, indicated by the white arrow, while canceling the interference of the previous bit blocks. The information rate for the SIC detector (46) is a lower bound on (20):

$$\begin{aligned} I_n(\mathbf{V}; \mathbf{Y}) &= \frac{1}{n} \sum_{s,l} H(b_l(\mathbf{V}_s)) - H(b_l(\mathbf{V}_s)|\mathbf{Y}, \mathbf{V}_1^{s-1}, b_1^{l-1}(\mathbf{V}_s)) \\ &\geq \frac{1}{S} \sum_{s,l} \frac{1}{\Gamma} \sum_t H(b_l(V_{s,t})) - H(b_l(V_{s,t})|\mathbf{Y}, \mathbf{V}_1^{s-1}, b_1^{l-1}(\mathbf{V}_s)) \\ &:= I_{n,\text{b-SIC}}. \end{aligned} \quad (47)$$

The limiting rate $I_{\text{b-SIC}} = \lim_{n \rightarrow \infty} I_{n,\text{b-SIC}}$ exists for stationary signalling and is an achievable rate for reliable communication. Since conditioning cannot increase entropy we have

$$I_{\text{MSD}} \leq I_{\text{b-SIC}}. \quad (48)$$

We remark that the rate (47) depends on the bit mapping.

VII. MISMATCHED DECODING

Implementing the FBA to compute symbol-wise APPs is challenging for channels with large memory \tilde{K} because the detection complexity grows exponentially with \tilde{K} . To limit complexity, we must usually consider a much smaller channel memory \tilde{N} . The main motivation for using a MCMC APP detector is that it can operate with a larger \tilde{N} than the FBA, as its complexity grows only quadratically with \tilde{N} , see Table I where the number of iterations refers to Sec. VIII.

The modified detector in [10] uses a conditionally Gaussian mismatched density with mean $\boldsymbol{\mu}_Q$ and covariance \mathbf{C}_{QQ} :

$$q(\mathbf{y}|\mathbf{u}) = \mathcal{N}(\mathbf{y} - |\boldsymbol{\Psi}'\tilde{\mathbf{x}}'|^{\circ 2}; \boldsymbol{\mu}_Q, \mathbf{C}_{QQ}) \quad (49)$$

where the Toeplitz channel matrix Ψ' is constructed from the time-reversed channel $\psi' = [\psi_{N-1}, \dots, \psi_0]^T$ with smaller memory $\tilde{N} = (N - 1)/2$ than the true system memory \tilde{K} , and $\tilde{\mathbf{x}}' = [\mathbf{s}_0, \mathbf{x}']^T$ where the channel input \mathbf{x}' is obtained by two-fold upsampling of $f_{\text{diff}}(\mathbf{u})$. We can control the receiver complexity by adjusting \tilde{N} .

If we focus on \mathbf{v} rather than \mathbf{u} , the auxiliary reverse channel is

$$Q(\mathbf{v}|\mathbf{y}) = \frac{q(\mathbf{y}|\mathbf{v})P(\mathbf{v})}{q(\mathbf{y})} \quad (50)$$

where $q(\mathbf{y})$ is obtained by marginalizing:

$$q(\mathbf{y}) = \sum_{\mathbf{v}} P(\mathbf{v})q(\mathbf{y}|\mathbf{v}). \quad (51)$$

The rate $I_{q,n}(\mathbf{V}; \mathbf{Y})$ via the auxiliary channel is a lower bound on $I_n(\mathbf{V}; \mathbf{Y})$ [10], [11], i.e., we have

$$I_n(\mathbf{V}; \mathbf{Y}) \geq I_{q,n}(\mathbf{V}; \mathbf{Y}) = \frac{1}{n} \mathbb{E} \left[\log_2 \frac{q(\mathbf{Y}|\mathbf{V})}{q(\mathbf{Y})} \right]. \quad (52)$$

The limiting rate $I_q(\mathcal{V}; \mathcal{Y}) = \lim_{n \rightarrow \infty} I_{q,n}(\mathbf{V}; \mathbf{Y})$ exists for stationary signalling and is an achievable rates for reliable communication with a receiver that uses $q(\mathbf{y}|\mathbf{v})$ rather than $p(\mathbf{y}|\mathbf{v})$ for JDD.

We next develop rate lower bounds for symbol-wise and bit-wise approximate APPs.

1) *Symbol-Wise Approximate APPs*: For detectors that compute *symbol-wise* APPs via the model (49) we have

$$\begin{aligned} I_{n,\text{SIC}} &\geq H_n(\mathbf{V}) + \frac{1}{n} \sum_s \sum_t \mathbb{E} [\log_2 Q(V_{s,t} | \mathbf{Y} \mathbf{V}_1^{s-1})] \\ &:= I_{q,n,\text{SIC}} \end{aligned} \quad (53)$$

where the inequality follows by using the same techniques as in [56, Eq. (39)] or [11, Eq. (37)-(41)]. Note that the bound also includes SDD ($S = 1$). The same rates as in (53) can be obtained by MSD since $I_{n,\text{MSD}} = I_{n,\text{SIC}}$, i.e., we have $I_{q,n,\text{MSD}} = I_{q,n,\text{SIC}}$. The required metrics can be computed by using the FBA (e.g., [21], [10, Sec. IV]) or Gibbs sampling. The limiting rate $I_{q,\text{SIC}} = \lim_{n \rightarrow \infty} I_{q,n,\text{SIC}}$ exists for stationary signalling and is an achievable rate for reliable communication with a receiver that uses the auxiliary metric $q(\mathbf{y}|\mathbf{v})$ for detection instead of the true channel likelihood $p(\mathbf{y}|\mathbf{v})$.

2) *Bit-Wise Approximate APPs*: Likewise, for detectors computing *bit-wise* APPs via the model (49) we have

$$\begin{aligned} I_{n,\text{b-SIC}} &\geq \\ &H_n(\mathbf{V}) + \frac{1}{n} \sum_{s,t} \mathbb{E} [\log_2 Q(b_l(V_{s,t}) | \mathbf{Y}, \mathbf{V}_1^{s-1}, b_1^{l-1}(\mathbf{V}_s))] \\ &:= I_{q,n,\text{b-SIC}}. \end{aligned} \quad (54)$$

The limiting rate $I_{q,\text{b-SIC}} = \lim_{n \rightarrow \infty} I_{q,n,\text{b-SIC}}$ again exists for stationary inputs and is an achievable rate for reliable communications. To maximize the achievable rates under mismatched decoding, we optimize $\mu_{\mathbf{Q}}$ and $\mathbf{C}_{\mathbf{Q}\mathbf{Q}}$ of the auxiliary channel (49) according to [10, Sec. III. C].

Parameter	Value
Block length	$n \geq 20 \times 10^3$ transmit symbols
Fiber length	$L \in \{0, 30 \text{ km}\}$
Carrier wavelength	1550 nm (C band)
CD parameter	$\beta_2 = -2.168 \times 10^{-23} \text{ s}^2/\text{km}$
Symbol rate	$B = 35 \text{ GBaud}$
Attenuation factor	0 dB/km
Oversampling factor	$N_{\text{os}} = 2$
FD-RC roll-off factor	$\alpha \in \{0, 0.2\}$

TABLE II: Simulation parameters based on SSMF.

Name	Alphabet
Unipolar M -PAM	$\mathcal{A} = \{0, 1, \dots, 2^m - 1\}$
Bipolar M -ASK	$\mathcal{A} = \{\pm 1, \pm 3, \dots, \pm(2^m - 1)\}$
M -SQAM (cf. [10])	$\mathcal{A} = \{\pm a \pm ja \mid a = 1, 2, \dots, M/4\}$

TABLE III: Modulation formats.

VIII. NUMERICAL RESULTS

This section provides numerical results for SDD and SIC receivers. Table II shows the simulation parameters. We use either $L = 0$ or $L = 30 \text{ km}$ of SSMF but we neglect fiber attenuation. The average transmit power is

$$P_{\text{tx}} = \frac{\mathbb{E} [\|X(t)\|^2]}{n \cdot T_s} \quad (55)$$

and the variance of the noise samples after filtering is $\sigma_N^2 = 1$ so we define $\text{SNR} := P_{\text{tx}}$. We use the modulation formats and alphabets from Tab. III, where $m = \log_2 M$. The spectral efficiency (SE) of FD-RC pulses with roll-off factor α is

$$\text{SE} = \frac{R}{(1 + \alpha)} \quad [\text{bit/s/Hz}] \quad (56)$$

where R is the information rate in bpcu. We estimate R by computing $I_q(\mathcal{V}; \mathcal{Y})$, $I_{q,\text{SIC}}$ and $I_{q,\text{b-SIC}}$ via Monte Carlo simulation, see [10], [11].

A. SIC rates via FBA

We use the FBA to compute the auxiliary metrics in Sec. VII when the complexity is feasible. Fig. 7 and Fig. 8 show the JDD rates $I_q(\mathcal{U}; \mathcal{Y})$ and SIC rates $I_{q,\text{SIC}}$ for M -PAM, M -ASK and M -SQAM modulation and $L = 30 \text{ km}$ of fiber. The auxiliary channel memory is $\tilde{N} = 9$ and $\tilde{N} = 7$ for $M = 4$ and $M = 8$, respectively. The rates increase with the number of SIC stages S .

First, note that $\tilde{N} = 9$ suffices for SDD, SIC, and JDD to achieve nearly 2 bpcu for all 4-ary modulations and large SNRs. For JDD this was observed in [10, Fig. 8a]. Fig. 7 suggests that SDD is nearly rate-optimal for large SNRs and SIC is not required, i.e., the channel outputs provide sufficient statistics to estimate the data via the auxiliary channel (see [10, Fig. 1] for BSPK and no noise). For medium SNRs, SDD shows larger losses for constellations with phases, i.e., ASK and SQAM.

For 8-ary modulations and $\tilde{N} = 7$, the rates are limited by interference and saturate before 3 bpcu. Higher rates can be achieved by increasing \tilde{N} . Likewise, for medium SNRs, SDD

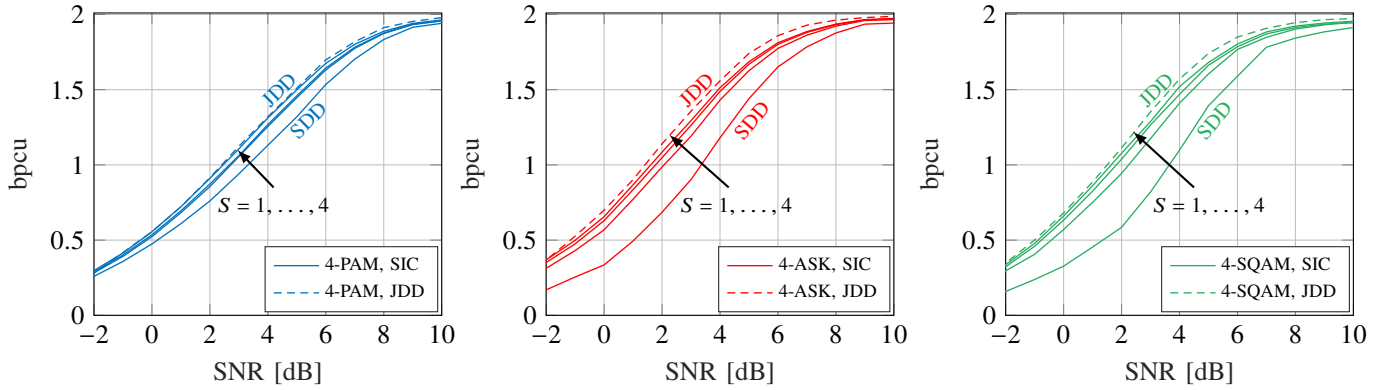


Fig. 7: SIC rates for 4-PAM/ASK, QPSK, $\tilde{N} = 9$, sinc pulses and $L = 30$ km of fiber.

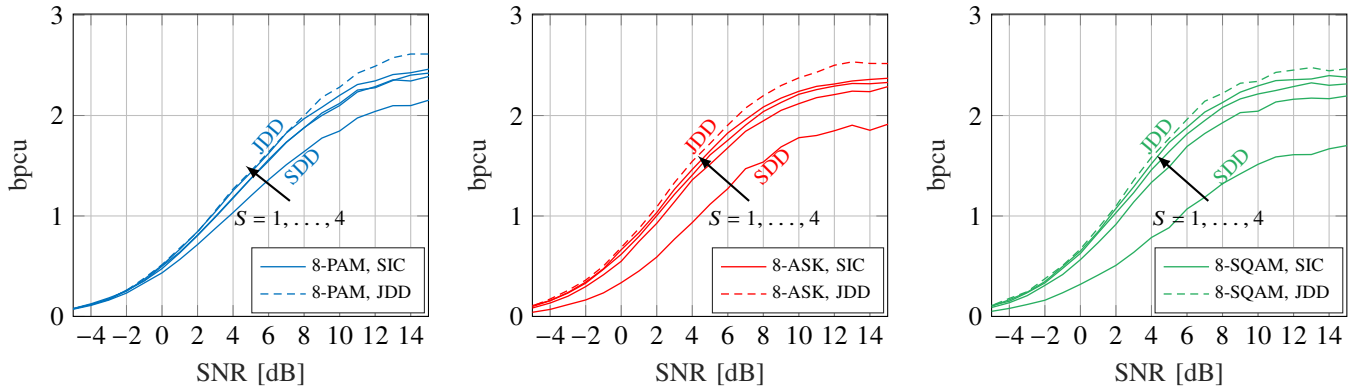


Fig. 8: SIC rates for 8-PAM/ASK, 8-SQAM, $\tilde{N} = 7$, sinc pulses and $L = 30$ km of fiber.

shows even larger losses for ASK and 8-SQAM as compared to JDD; this is due to the small auxiliary memory.

Both figures show that SIC substantially improves SDD and can approach the JDD rates for large S . The performance with $S = 4$ stages agrees well with the JDD rate at low-to-medium SNR. For sufficiently large S we achieve roughly the same energy gains for bipolar ASK, unipolar PAM and complex SQAM as in [10].

B. Polar-Coded SDD and SIC with the FBA

We show that the SIC rates from Fig. 7 and Fig. 8 can be achieved by practical communication systems with FEC. We use polar codes [57] that easily adapt to MLC/MSD [58]. In addition, we use successive cancellation list (SCL) decoding [48] that passes a list of the most likely codewords between stages. The detector of the next stage uses this list to generate a list of APPs for the next decoder [49], [50], i.e., we pass a list of possible bit strings to the next stage instead of passing only one hard-decision string.

We simulate 10^6 frames that each have 2^{10} 4-PAM/ASK symbols. For MSD with 4-ASK/PAM (2 bit-levels), we use $2S$ polar codes of length $2048/(2S)$ bits each. We set the information rate (29) to $R = 1$ bpcu, i.e., there are $k = 1024$ information bits per transmitted frame. The spectral efficiency is thus $SE \approx 0.83$ bit/s/Hz. The SCL list size is 8 and we

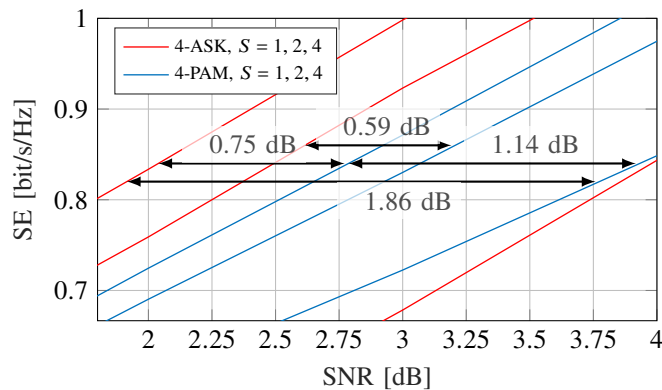
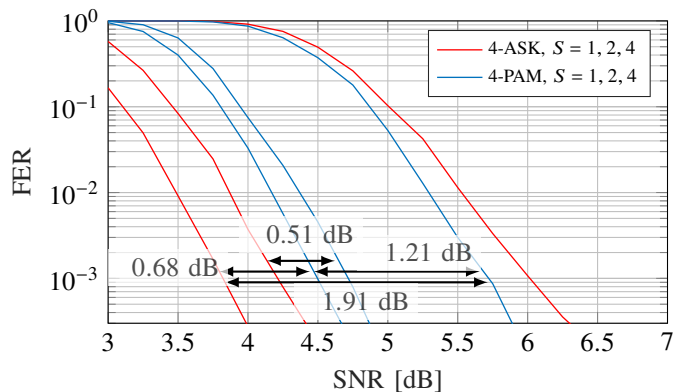
use an outer 16-bit cyclic redundancy check (CRC) code, as explained in [48]. The polar codes are designed using Monte Carlo methods [57], [59] and the code rate of all component codes (S SIC levels, m bit levels) is simultaneously optimized.

Fig. 9a shows $I_{q,SIC}$ for $\tilde{N} = 5$ and FD-RC with $\alpha = 0.2$. For SDD, the 4-ASK and 4-PAM rates almost coincide. Using SIC with $S = 2, 4$, ASK gains approximately 0.59 dB and 0.75 dB in SNR over PAM, respectively, at a SE of 0.83 bit/s/Hz. Comparing SIC with $S = 4$ to SDD ($S = 1$), PAM and ASK gain 1.14 dB and 1.86 dB in SNR, respectively. Fig. 9b shows the FERs for which the SNR gains closely match those of Fig. 9a at FER 10^{-3} .

C. SIC rates via Gibbs sampling

This section provides numerical results for $I_{q,b,SIC}$ in (54) where the APPs are approximated via Gibbs sampling. The results are compared to $I_{q,SIC}$ where the APPs are computed via the FBA.

To avoid stalling at high SNR, we use $N_{\text{par}} = 20$ parallel Gibbs samplers and perform $N_{\text{iter}} = 60$ iterations per Gibbs sampler. The first few iterations (here ten) are commonly referred to as the burn-in period, and are discarded for estimating the APPs. For every SNR, we use a training set of 10×10^3 symbols to optimize the confidence parameter η (42) with respect to $I_{q,b,SIC}$. This optimization is carried out via a

(a) Achievable rates around $SE \approx 0.83$ bit/s/Hz.(b) FER at a $SE \approx 0.83$ bit/s/Hz for polar codes with block length $n = 2048/(2S)$, multistage list decoding with list size 8 and outer 16-CRC code.Fig. 9: SE and polar-coded FER for 4-ASK/PAM, $\tilde{N} = 5$, FD-RC ($\alpha = 0.2$) and $L = 30$ km of fiber.

line-search. We use a binary reflected Gray code to label the elements in the alphabet \mathcal{A} .

Fig. 10 shows results for $L = 30$ km and sinc pulses (cf. Fig. 7, 8) and plots the SIC rates $I_{q,b-SIC}$ for 4-ASK, 8-ASK and $S = 1, \dots, 4$, where the APPs are estimated via Gibbs sampling. In (48) we found that I_{b-SIC} is an upper bound on I_{SIC} , and for a sufficiently large auxiliary model memory this should also be reflected in Fig. 10. For $S = 1$ and low to medium SNRs, Fig. 10 shows that $I_{q,b-SIC} \geq I_{q,SIC}$. At high SNR, the Gibbs sampler still stalls and the rates saturate. Similar results are obtained for PAM or SQAM when comparing $I_{q,SIC}$ computed via the FBA to $I_{q,b-SIC}$ computed via Gibbs sampling. These results are omitted.

As S increases, the rates $I_{q,b-SIC}$ via Gibbs sampling approach the JDD curve at low and medium SNRs. At high SNR the JDD rate could not be reached. Possible remedies for this behavior might be more iterations, more parallel samplers or advanced Gibbs samplers that optimize the proposal distribution.

Fig. 11 shows the SIC rates with Gibbs sampling for M -ASK, M -PAM and M -SQAM for $M = 8, 16, 32$ and memory $\tilde{N} = 9$. In this case, complexity prohibits the use of FBA to create reference plots. ASK and PAM constellations achieve the highest possible SE of $\log_2 M/(1 + \alpha)$ for $M = 8, 16$. For $M = 32$ both curves saturate due to ISI and this can be resolved by using $\tilde{N} > 9$. ASK gains up to 2.6 dB over PAM for $M = 32$. M -SQAM saturates at lower values for $M = 8, 16, 32$. Due to the structure of SQAM, there are more phase ambiguities and it is harder to distinguish the phases. More knowledge about the interference (larger \tilde{N}) can help to improve the performance. Another option is optimizing complex constellations since SQAM or QAM have symmetries that cause many phase ambiguities.

The asymptotic complexity of b-SIC via Gibbs sampling and SIC via the FBA is compared in Tab. I in terms of the number of multiplication. The cost of both algorithms scales linearly with the block length n and the number of SIC stages S . The FBA complexity grows exponentially with the number

of channel taps, while the Gibbs sampling complexity grows quadratically. The number of iterations for Gibbs sampling can be reduced to reduce the computational cost.

Fig. 12 shows the SIC rates for $S = 4$ stages and 4-ASK when using Gibbs sampling with $N_{iter} = 1, 2, 5, 10, 20$ iterations after the burn-in period. Observe that more iterations are required for high SNRs and that the number of iterations can be reduced at the cost of only slightly lower rates.

IX. CONCLUSION

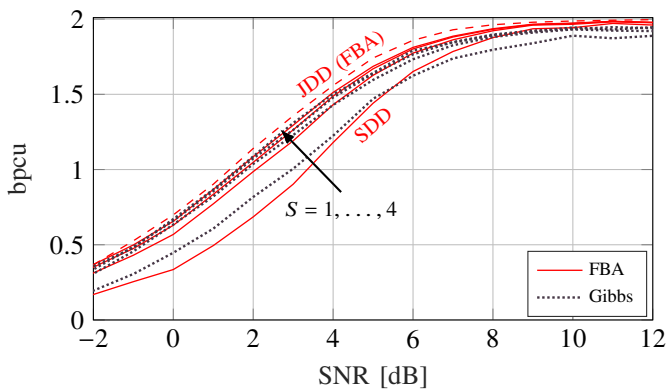
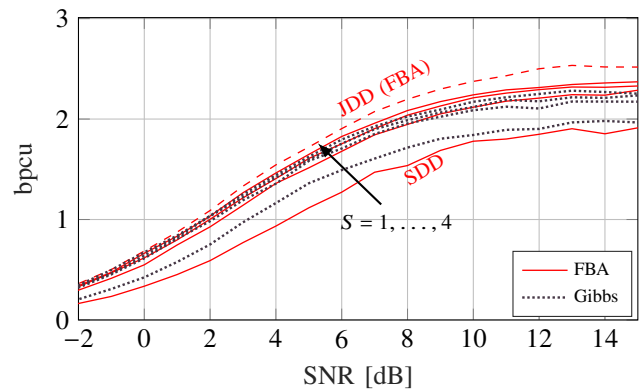
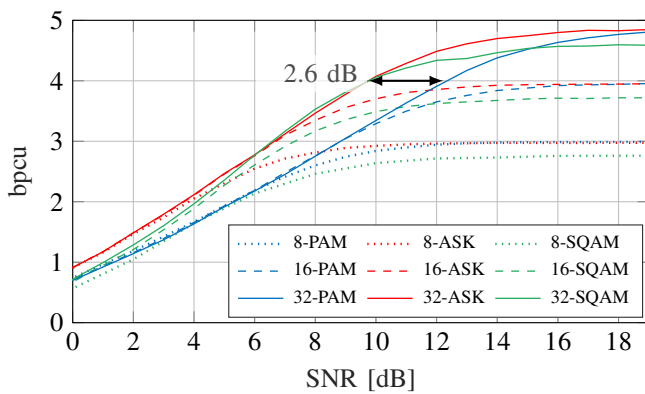
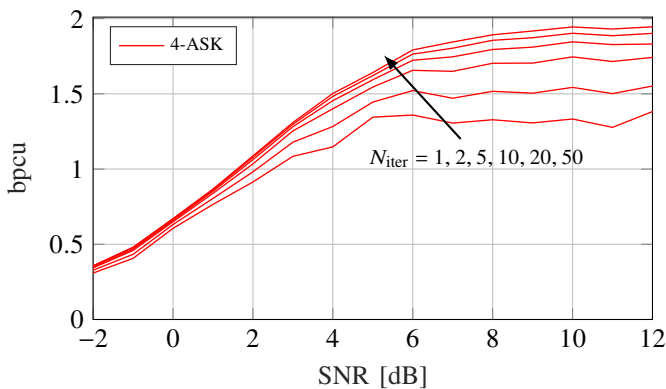
Two simplified transceiver architectures were studied for direct detection (DD) receivers with two-fold oversampling: SDD and SIC. We showed that SDD can exhibit large rate loss as compared to JDD, especially for BM. We proposed SIC with MLC/MSD to mitigate the rate loss and showed that only a few SIC stages are needed to approach the JDD performance. Simulations with polar codes verified the information rate computations and showed that BM can significantly outperform intensity modulation (IM) for practical receivers and DD.

To reduce the detector complexity, we proposed using Gibbs sampling. Simulations at low-to-intermediate SNRs showed that only a few Gibbs iterations achieve rates close to the JDD rates.

There are many open research problems. For example, symmetric complex-valued constellations suffer from phase ambiguities which motivates using asymmetric constellations or probabilistic constellation shaping. One might also consider different pulse shapes and precoding techniques. Gibbs sampling can help to speed up the optimization. Gibbs sampling might be further optimized in the high SNR regime to minimize the effects of stalling.

ACKNOWLEDGMENT

The authors wish to thank G. Böcherer, T. Rahman and N. Stojanović for useful suggestions and discussions.

(a) 4-ASK, $\tilde{N} = 9$.(b) 8-ASK, $\tilde{N} = 7$.Fig. 10: Comparison of SIC rates via Gibbs sampling and FBA for sinc pulses and $L = 30$ km of fiber.Fig. 11: SIC rates via Gibbs sampling using FD-RC ($\alpha = 0.2$) pulses, $L = 0$ km and $S = 4$.Fig. 12: SIC rates via Gibbs sampling vs. number of Gibbs sampler iterations for 4-ASK, $S = 4$ and $N_{\text{par}} = 20$ parallel samplers.

APPENDIX

A. Phase Ambiguities in Symbol-Wise APPs

For u.i.i.d. channel inputs, one obtains the symbol-wise APPs $P(x_\kappa|\mathbf{y})$ via [10, Eq. (55)]:

$$P(x_\kappa|\mathbf{y}) = \frac{1}{A} \sum_{\mathbf{x}_{\setminus x_\kappa}} \mathcal{N}(\mathbf{y} - |\Psi\mathbf{x}'|^2) \quad (57)$$

where A is a normalization factor. Consider an all-zeros initial channel state vector \mathbf{s}_0 . We multiply $\tilde{\mathbf{x}}$ by a complex scalar $e^{j\phi}$, $\phi \in [0, 2\pi)$, without changing (57):

$$\begin{aligned} P_{X_\kappa|Y}(a|\mathbf{y}) &= \frac{1}{A} \sum_{\substack{\tilde{\mathbf{x}}^n \in \tilde{\mathcal{A}}^n \\ \tilde{x}_\kappa = a}} \mathcal{N}(\mathbf{y} - |\Psi(\tilde{\mathbf{x}}' e^{j\phi})|^2) \\ &= \frac{1}{A} \sum_{\substack{\tilde{\mathbf{x}}^n \in \tilde{\mathcal{A}}^n \\ \tilde{x}_\kappa = a \cdot e^{j\phi}}} \mathcal{N}(\mathbf{y} - |\Psi\tilde{\mathbf{x}}|^2) \end{aligned}$$

and substituted $\check{x}_\kappa = \tilde{x}'_\kappa e^{j\phi}$ and $\check{\mathcal{A}} = \{w e^{j\phi} | w \in \mathcal{A}\}$ in the last step. If the alphabet \mathcal{A} is rotationally invariant with respect to a given angle ϕ , i.e., $\check{\mathcal{A}} = \mathcal{A}$, we obtain

$$\begin{aligned} P_{X_\kappa|Y}(a|\mathbf{y}) &= \frac{1}{A} \sum_{\substack{\check{\mathbf{x}}^n \in \check{\mathcal{A}}^n \\ \check{x}_\kappa = a \cdot e^{j\phi}}} \mathcal{N}(\mathbf{y} - |\Psi\check{\mathbf{x}}|^2) \\ &= P_{X_\kappa|Y}(a e^{j\phi}|\mathbf{y}). \end{aligned}$$

and conclude that regardless of the channel Ψ , the symbol-wise APPs are phase ambiguous with respect to ϕ .

B. Differential Phase Coding for M -SQAM

A differential phase mapping for M -SQAM (cf. Tab. III) with $F = 4$ phases is shown in Fig. 13. The function $\text{circ}(\mathbf{a})$ generates an $F \times F$ circulant matrix from the vector \mathbf{a}^F that describes the phase inputs $\angle U_\kappa$ for transition from state $\angle X_{\kappa-1}$ to state $\angle X_\kappa$.

REFERENCES

- [1] M. Chagnon, "Optical communications for short reach," *J. Lightw. Technol.*, vol. 37, no. 8, pp. 1779–1797, April 2019.
- [2] S. D. Dissanayake and J. Armstrong, "Comparison of ACO-OFDM, DCO-OFDM and ADO-OFDM in IM/DD systems," *J. Lightw. Technol.*, vol. 31, no. 7, pp. 1063–1072, 2013.
- [3] L. Chen, B. Krongold, and J. Evans, "Performance analysis for optical OFDM transmission in short-range IM/DD systems," *J. Lightw. Technol.*, vol. 30, no. 7, pp. 974–983, 2012.
- [4] A. Mecozzi and M. Shttaif, "On the capacity of intensity modulated systems using optical amplifiers," *IEEE Photon. Technol. Lett.*, vol. 13, no. 9, pp. 1029–1031, 2001.
- [5] —, "Information capacity of direct detection optical transmission systems," *J. Lightw. Technol.*, vol. 36, no. 3, pp. 689–694, 2018.

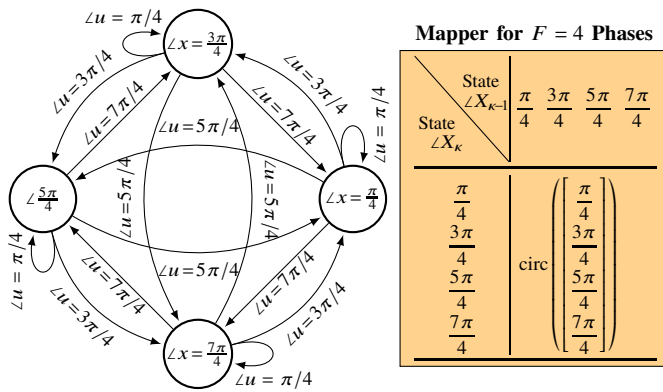


Fig. 13: Differential phase mapping for M -SQAM [41, Fig. 6].

- [6] M. Secondini and E. Forestieri, "Direct detection of bipolar pulse amplitude modulation," *J. Lightw. Technol.*, vol. 38, no. 21, pp. 5981–5990, 2020.
- [7] A. Tasbihi and F. R. Kschischang, "On the capacity of waveform channels under square-law detection of time-limited signals," *IEEE Trans. Inf. Theory*, vol. 66, no. 11, pp. 6682–6687, 2020.
- [8] —, "Direct detection under Tukey signalling," *J. Lightw. Technol.*, vol. 39, no. 21, pp. 6845–6857, 2021.
- [9] A. Mecozzi, C. Antonelli, and M. Shtaif, "Kramers–Kronig coherent receiver," *Optica*, vol. 3, no. 11, pp. 1220–1227, Nov 2016.
- [10] D. Plabst, T. Prinz, T. Wiegart, T. Rahman, N. Stojanović, S. Calabrò, N. Hanik, and G. Kramer, "Achievable rates for short-reach fiber-optic channels with direct detection," *J. Lightw. Technol.*, vol. 40, no. 12, pp. 3602–3613, 2022.
- [11] D. M. Arnold, H.-A. Loeliger, P. O. Vontobel, A. Kavčić, and W. Zeng, "Simulation-based computation of information rates for channels with memory," *IEEE Trans. Inf. Theory*, vol. 52, no. 8, pp. 3498–3508, 2006.
- [12] A. Sheikh, A. G. i. Amat, and G. Liva, "Achievable information rates for coded modulation with hard decision decoding for coherent fiber-optic systems," *J. Lightw. Technol.*, vol. 35, no. 23, pp. 5069–5078, 2017.
- [13] G. Liga, A. Alvarado, E. Agrell, and P. Bayvel, "Information rates of next-generation long-haul optical fiber systems using coded modulation," *J. Lightw. Technol.*, vol. 35, no. 1, pp. 113–123, 2017.
- [14] C. Douillard, M. Jézéquel, C. Berrou, D. Electronique, A. Picart, P. Didier, and A. Glavieux, "Iterative correction of intersymbol interference: turbo-equalization," *Eur. Trans. Telecommun.*, vol. 6, no. 5, pp. 507–511, 1995.
- [15] X. Wang and H. V. Poor, "Iterative (turbo) soft interference cancellation and decoding for coded CDMA," *IEEE Trans. Commun.*, vol. 47, no. 7, pp. 1046–1061, 1999.
- [16] U. Wachsmann, R. F. Fischer, and J. B. Huber, "Multilevel codes: Theoretical concepts and practical design rules," *IEEE Trans. Inf. Theory*, vol. 45, no. 5, pp. 1361–1391, 1999.
- [17] H. Pfister, J. Soriaga, and P. Siegel, "On the achievable information rates of finite state ISI channels," in *IEEE Global Telecommun. Conf.*, vol. 5, 2001, pp. 2992–2996 vol.5.
- [18] J. B. Soriaga, H. D. Pfister, and P. H. Siegel, "Determining and approaching achievable rates of binary intersymbol interference channels using multistage decoding," *IEEE Trans. Inf. Theory*, vol. 53, no. 4, pp. 1416–1429, 2007.
- [19] R. Müller and W. Gerstacker, "On the capacity loss due to separation of detection and decoding," *IEEE Trans. Inf. Theory*, vol. 50, no. 8, pp. 1769–1778, 2004.
- [20] S. Ten Brink, G. Kramer, and A. Ashikhmin, "Design of low-density parity-check codes for modulation and detection," *IEEE Trans. Commun.*, vol. 52, no. 4, pp. 670–678, 2004.
- [21] L. Bahl, J. Cocke, F. Jelinek, and J. Raviv, "Optimal decoding of linear codes for minimizing symbol error rate," *IEEE Trans. Inf. Theory*, vol. 20, no. 2, pp. 284–287, 1974.
- [22] S. M. Kay, *Fundamentals of Statistical Signal Processing*. Prentice-Hall, Inc., 1993.
- [23] D. J. C. MacKay, *Information Theory, Inference and Learning Algorithms*. Cambridge University Press, 2003.
- [24] V. Buchoux, O. Cappé, and É. Moulines, "Turbo multiuser detection for coded DS-SS systems: A Gibbs sampling approach," in *Asilomar Conf. Signals, Sys., Computers*, vol. 2, 2000, pp. 1426–1430.
- [25] X. Wang and R. Chen, "Adaptive Bayesian multiuser detection for synchronous CDMA with Gaussian and impulsive noise," *IEEE Trans. Signal Process.*, vol. 48, no. 7, pp. 2013–2028, 2000.
- [26] T. M. Schmidl, A. Gatherer, X. Wang, and R. Chen, "Interference cancellation using the Gibbs sampler," in *Vehicular Technology Conference Fall 2000*, vol. 1. IEEE, 2000, pp. 429–433.
- [27] Z. Shi, H. Zhu, and B. Farhang-Boroujeny, "Markov chain Monte Carlo techniques in iterative detectors: a novel approach based on Monte Carlo integration," in *IEEE Global Telecommun. Conf.*, vol. 1. IEEE, 2004, pp. 325–329.
- [28] Z. Yang and X. Wang, "Turbo equalization for GMSK signaling over multipath channels based on the Gibbs sampler," *IEEE J. Sel. Areas Commun.*, vol. 19, no. 9, pp. 1753–1763, 2001.
- [29] B. Farhang-Boroujeny, H. Zhu, and Z. Shi, "Markov chain Monte Carlo algorithms for CDMA and MIMO communication systems," *IEEE Trans. Signal Process.*, vol. 54, no. 5, pp. 1896–1909, 2006.
- [30] R.-H. Peng, R.-R. Chen, and B. Farhang-Boroujeny, "Markov chain Monte Carlo detectors for channels with intersymbol interference," *IEEE Trans. Signal Process.*, vol. 58, no. 4, pp. 2206–2217, 2009.
- [31] —, "Low complexity Markov chain Monte Carlo detector for channels with intersymbol interference," in *IEEE Int. Conf. Commun.*, 2009, pp. 1–5.
- [32] F. M. Kashif, H. Wymeersch, and M. Z. Win, "Monte Carlo equalization for nonlinear dispersive satellite channels," *IEEE J. Sel. Areas Commun.*, vol. 26, no. 2, pp. 245–255, 2008.
- [33] X. Mao, P. Amini, and B. Farhang-Boroujeny, "Markov chain Monte Carlo MIMO detection methods for high signal-to-noise ratio regimes," in *IEEE Global Telecommun. Conf.*, 2007, pp. 3979–3983.
- [34] M. Hansen, B. Hassibi, A. G. Dimakis, and W. Xu, "Near-optimal detection in MIMO systems using Gibbs sampling," in *IEEE Global Telecommun. Conf.*, 2009, pp. 1–6.
- [35] M. Senst and G. Ascheid, "A Rao-Blackwellized Markov chain Monte Carlo algorithm for efficient MIMO detection," in *IEEE Int. Conf. Commun. (ICC)*. IEEE, 2011, pp. 1–6.
- [36] B. Hassibi, M. Hansen, A. G. Dimakis, H. A. J. Alshamary, and W. Xu, "Optimized Markov chain Monte Carlo for signal detection in MIMO systems: An analysis of the stationary distribution and mixing time," *IEEE Trans. Signal Process.*, vol. 62, no. 17, pp. 4436–4450, 2014.
- [37] J. C. Hedstrom, C. H. Yuen, R.-R. Chen, and B. Farhang-Boroujeny, "Achieving near MAP performance with an excited Markov chain Monte Carlo MIMO detector," *IEEE Trans. Wireless Commun.*, vol. 16, no. 12, pp. 7718–7732, 2017.
- [38] G. Agrawal, *Fiber-Optic Communication Systems*, 4th ed. John Wiley & Sons, Inc., Hoboken, NJ, USA, 2010.
- [39] R.-J. Essiambre, G. Kramer, P. J. Winzer, G. J. Foschini, and B. Goebel, "Capacity limits of optical fiber networks," *J. Lightw. Technol.*, vol. 28, no. 4, pp. 662–701, 2010.
- [40] D. Plabst, F. J. García-Gómez, T. Wiegart, and N. Hanik, "Wiener filter for short-reach fiber-optic links," *IEEE Commun. Lett.*, vol. 24, no. 11, pp. 2546–2550, 2020.
- [41] L. Schmalen, S. ten Brink, and A. Leven, "Advances in detection and error correction for coherent optical communications: Regular, irregular, and spatially coupled LDPC code designs," *CoRR*, vol. abs/1704.04618, 2017. [Online]. Available: <http://arxiv.org/abs/1704.04618>
- [42] J. Huber, "Trelliscodierte digitale Übertragungsverfahren," in *Trelliscodierung*. Springer, 1992, pp. 141–260.
- [43] F. Schuh, A. Schenk, and J. B. Huber, "Reduced complexity super-trellis decoding for convolutionally encoded transmission over ISI-channels," in *2013 Int. Conf. Computing, Networking, and Commun. (ICNC)*, 2013, pp. 484–489.
- [44] T. R. Giallorenzi and S. G. Wilson, "Multiuser ML sequence estimator for convolutionally coded asynchronous DS-SS systems," *IEEE Trans. Commun.*, vol. 44, no. 8, pp. 997–1008, 1996.
- [45] A. Kavčić, X. Ma, and M. Mitzenmacher, "Binary intersymbol interference channels: Gallager codes, density evolution, and code performance bounds," *IEEE Trans. Inf. Theory*, vol. 49, no. 7, pp. 1636–1652, 2003.
- [46] C. E. Shannon, "Probability of error for optimal codes in a gaussian channel," *Bell Sys. Techn. J.*, vol. 38, no. 3, pp. 611–656, 1959.
- [47] Y. Polyanskiy, H. V. Poor, and S. Verdú, "Channel coding rate in the finite blocklength regime," *IEEE Trans. Inf. Theory*, vol. 56, no. 5, pp. 2307–2359, 2010.
- [48] I. Tal and A. Vardy, "List decoding of polar codes," *IEEE Trans. Inf. Theory*, vol. 61, no. 5, pp. 2213–2226, 2015.

- [49] T. Prinz and P. Yuan, "Successive cancellation list decoding of BMERA codes with application to higher-order modulation," in *IEEE Int. Symp. Turbo Codes & Iterative Inf. Proc. (ISTC)*. IEEE, 2018, pp. 1–5.
- [50] L. Karakchieva and P. Trifonov, "Joint list multistage decoding with sphere detection for polar coded SCMA systems," in *ITG Conf. Sys., Commun. Coding*. VDE, 2019, pp. 1–6.
- [51] A. Martinez, A. G. i Fàbregas, G. Caire, and F. M. Willems, "Bit-interleaved coded modulation revisited: A mismatched decoding perspective," *IEEE Trans. Inf. Theory*, vol. 55, no. 6, pp. 2756–2765, 2009.
- [52] G. Caire, G. Taricco, and E. Biglieri, "Bit-interleaved coded modulation," *IEEE Trans. Inf. Theory*, vol. 44, no. 3, pp. 927–946, 1998.
- [53] H. Imai and S. Hirakawa, "A new multilevel coding method using error-correcting codes," *IEEE Trans. Inf. Theory*, vol. 23, no. 3, pp. 371–377, 1977.
- [54] H. Zhu, B. Farhang-Boroujeny, and R.-R. Chen, "On performance of sphere decoding and Markov chain Monte Carlo detection methods," *IEEE Signal Process. Lett.*, vol. 12, no. 10, pp. 669–672, 2005.
- [55] D. Auras, U. Deidersen, R. Leupers, and G. Ascheid, "VLSI design of a parallel MCMC-based MIMO detector with multiplier-free Gibbs samplers," in *Int. Conf. Very Large Scale Integration*, 2014, pp. 1–6.
- [56] P. Sadeghi, P. O. Vontobel, and R. Shams, "Optimization of information rate upper and lower bounds for channels with memory," *IEEE Trans. Inf. Theory*, vol. 55, no. 2, pp. 663–688, 2009.
- [57] E. Arıkan, "Channel polarization: A method for constructing capacity-achieving codes for symmetric binary-input memoryless channels," *IEEE Trans. Inf. Theory*, vol. 55, no. 7, pp. 3051–3073, 2009.
- [58] M. Seidl, A. Schenk, C. Stierstorfer, and J. B. Huber, "Polar-coded modulation," *IEEE Trans. Commun.*, vol. 61, no. 10, pp. 4108–4119, 2013.
- [59] G. Böcherer, T. Prinz, P. Yuan, and F. Steiner, "Efficient polar code construction for higher-order modulation," in *IEEE Wireless Commun. Networking Conf. Workshops (WCNCW)*, 2017, pp. 1–6.